Forces drive basement membrane invasion in *Caenorhabditis elegans*

Rodrigo Cáceres[a,b,c], Nagagireesh Bojanala[a,c], Laura C. Kelley[d], Jes Dreier[e], John Manzi[a,c], Fahima Di Federico[a,c], Qiuyi Chi[d], Thomas Risler[a,c], Ilaria Testa[e], David R. Sherwood[d], and Julie Plastino[a,c,1]

[a]Laboratoire Physico-Chimie Curie, Institut Curie, PSL Research University, CNRS, 75005 Paris, France; [b]Université Paris Descartes, 75005 Paris, France; [c]Sorbonne Université, 75005 Paris, France; [d]Department of Biology, Regeneration Next, Duke University, Durham, NC 27705; and [e]Department of Applied Physics and Science for Life Laboratory, KTH Royal Institute of Technology, 10014 Stockholm, Sweden

Edited by Thomas D. Pollard, Yale University, New Haven, CT, and approved October 1, 2018 (received for review May 24, 2018)

During invasion, cells breach basement membrane (BM) barriers with actin-rich protrusions. It remains unclear, however, whether actin polymerization applies pushing forces to help break through BM, or whether actin filaments play a passive role as scaffolding for targeting invasive machinery. Here, using the developmental event of anchor cell (AC) invasion in *Caenorhabditis elegans*, we observe that the AC deforms the BM and underlying tissue just before invasion, exerting forces in the tens of nanonewtons range. Deformation is driven by actin polymerization nucleated by the Arp2/3 complex and its activators, whereas formins and cross-linkers are dispensable. Delays in invasion upon actin regulator loss are not caused by defects in AC polarity, trafficking, or secretion, as appropriate markers are correctly localized in the AC even when actin is reduced and invasion is disrupted. Overall force production emerges from this study as one of the main tools that invading cells use to promote BM disruption in *C. elegans*.

actin cytoskeleton | force production | cell invasion | Arp2/3 complex | anchor cell

Basement membrane (BM) is a sheet of specialized extracellular matrix that separates different tissue compartments. Because of the small pore size of BMs, the movement of cells across BM barriers does not occur by normal migration, but by a distinct process known as invasion. Invasive cancer cells derived from epithelia make holes in BM using actin-rich protrusions at the cell leading edge called invadopodia, which secrete matrix metalloproteases to digest extracellular matrix fibers (1–3). Despite the presence of actin in invasive protrusions, it is unclear whether actin polymerization produces forces that help pierce BM or whether actin simply serves as a scaffold for trafficking and clustering of invasive components, including proteases, to the invasive cell membrane (4, 5). Actin-based force production is required for postbreach motility in the stroma underlying the BM (6, 7); however, the role of mechanical forces in the initial stages of BM disruption has not been addressed. Because BM penetration is a key step in metastasis, a physical understanding of invasion could be useful for designing novel strategies for metastasis inhibition.

Here we look at the role of force production in BM invasion, using a developmental model of cell invasion: anchor cell (AC) invasion in *Caenorhabditis elegans*. AC invasion resembles, in many respects, an invading cancer cell (8) but can be observed in its native environment because of the ease of imaging and genetic manipulation in the worm.

Results and Discussion

The Experimental System. Toward the end of larval development in *C. elegans*, a single uterine cell, the AC, makes an opening in the BM that separates the uterus from the underlying layer of epithelial cells, the vulval precursor cells (VPCs), thus initiating vulva formation. The invasion of the AC is synchronized with the divisions of the descendants of P6.p, a VPC that lies just under the AC on the other side of the BM. Invasion occurs between the P6.p 2-cell and 4-cell stage (i.e., between the first division of P6.p and the subsequent division of P6.p daughters). By the early to middle P6.p 4-cell stage, about 60 min after initiation of invasion, all WT worms clear a gap in the BM the width of the AC (Fig. 1*A*).

At the late P6.p 2-cell stage, a side view of the AC shows that F-actin localizes to the invasive AC membrane that is juxtaposed to the BM (Fig. 1*B*). The actin protrusion enlarges in size and density as a hole forms and widens, and then retracts once the BM hole reaches the border of the AC (Fig. 1*B*). The coincidence of actin accumulation and BM degradation is reminiscent of cancer cell invadopodia, as is the fact that the AC expresses zinc matrix metalloproteases during invasion that could potentially degrade BM (9, 10). Unlike invasive cancer cells, the apical side of the AC remains attached to the surrounding uterine cells, and only the basal actin protrusion crosses the BM and then withdraws. AC invasion therefore mimics the first stage of cancer cell invasion, where BM is broken by an actin-filled protrusion, without the confounding effects of subsequent motility.

The Invading AC Applies Force with an Actin-Filled Protrusion. At the late P6.p 2-cell stage, just before the initial BM break occurred, we observed that the BM and underlying tissue were deformed beneath the actin-rich invasive cell membrane of the AC, displaying indentations 1.1 ± 0.3 μm deep on average ($n = 36$; Fig. 1 *C* and *D*). Deformations such as those observed under the AC

Significance

Basement membrane is a particular kind of sheet-like extracellular matrix that separates tissue compartments. Invasion of cells through basement membrane barriers is a key aspect of many normal and pathological processes, including organ development and cancer cell metastasis. Invasive protrusions are rich in actin, a cytoskeletal biopolymer, the self-assembly of which can produce force and remodel extracellular matrix. However, in the invasive protrusion, actin has been attributed a function in scaffolding and trafficking, and its mechanical role has not been explored. Here we show that invading cells in *C. elegans* apply forces via actin assembly to break through basement membrane, and that force production is one of the key features of invasion.

Author contributions: R.C., I.T., D.R.S., and J.P. designed research; R.C., N.B., L.C.K., J.D., and J.P. performed research; R.C., N.B., L.C.K., J.M., F.D.F., Q.C., T.R., I.T., and J.P. contributed new reagents/analytic tools; R.C., N.B., L.C.K., J.D., and J.P. analyzed data; and T.R., I.T., D.R.S., and J.P. wrote the paper.

The authors declare no conflict of interest.

This article is a PNAS Direct Submission.

[1]To whom correspondence should be addressed. Email: julie.plastino@curie.fr.

This article contains supporting information online at www.pnas.org/lookup/suppl/doi:10.1073/pnas.1808760115/-/DCSupplemental.

Published online October 22, 2018.

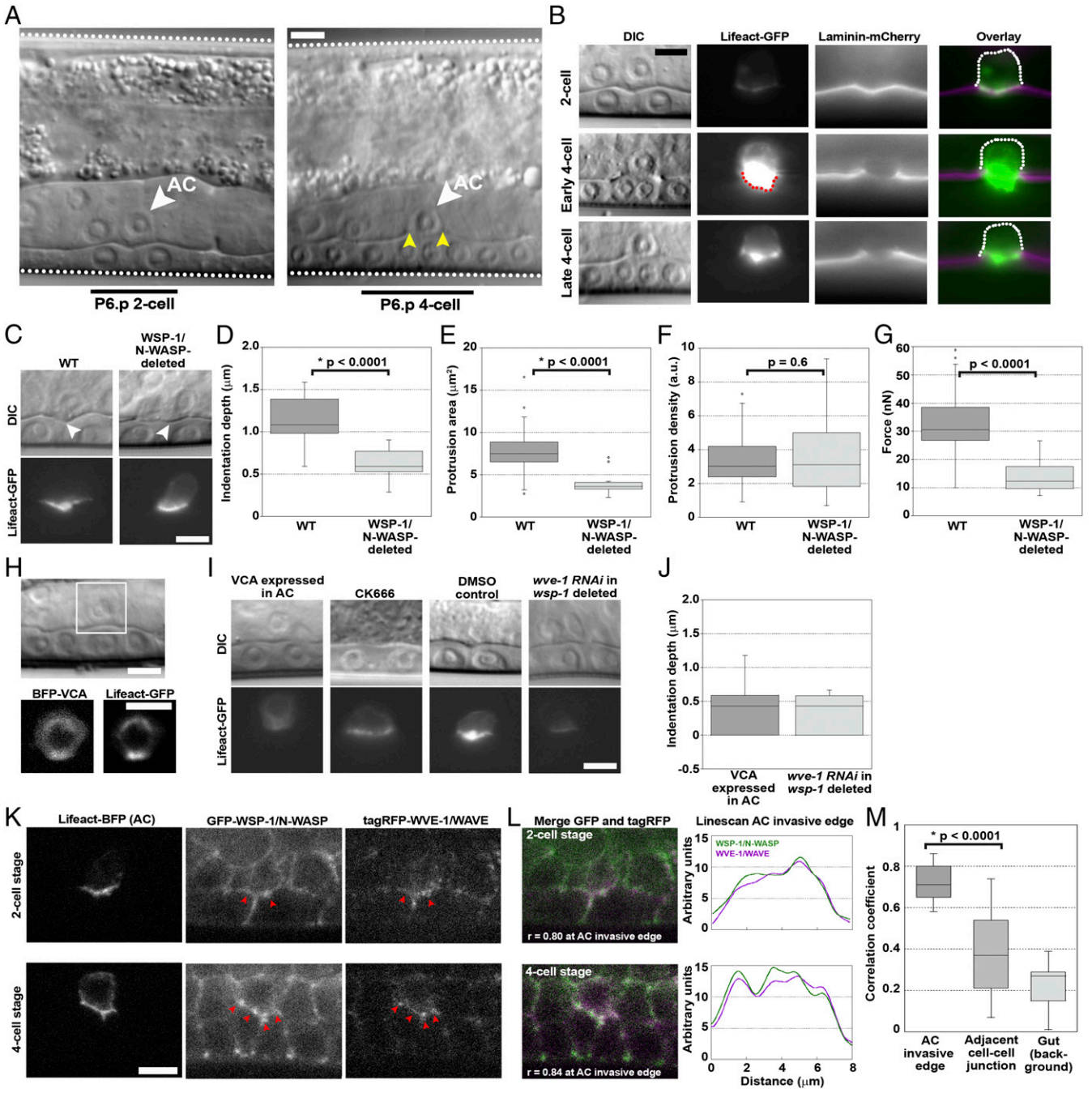

Fig. 1. The invading AC exerts force via an Arp2/3 complex-dependent protrusion, dependent on both WSP-1/N-WASP and WVE-1/WAVE. (*A*) AC invasion as viewed by DIC microscopy. The AC (white arrowheads), the body wall of the worm (white dotted lines), P6.p 2-cell and 4-cell stage (black bars) and the break in the phase dense line of the BM (yellow arrowheads) are marked. (*B*) Actin in the protrusion, observed by AC-specific expression of Lifeact-GFP over the course of invasion of the BM, observed by laminin-mCherry. Scaling is not adjusted in the single-channel images, showing the increase of F-actin in the AC (red dotted line). Once the BM gap is as wide as the AC, at the late P6.p 4-cell stage, the protrusion diminishes and retracts. The back of the cell is immobile (dotted white line). (*C*) The AC indents the BM (white arrowheads) before invasion, with an actin-rich protrusion. WSP-1/N-WASP deletion reduces the indentation depth and the actin protrusion size, although the density remains unchanged. (*D*–*F*) Quantification of indentation depths, and the sizes and densities of actin protrusions. (*G*) Estimated forces produced by the AC in WT and WSP-1/N-WASP-deleted conditions. (*H*) The VCA domain of WSP-1/N-WASP, labeled with BFP and expressed specifically in the AC, completely blocks invasion and perturbs actin protrusion formation. (*I*) Sample images of indentations and actin protrusions under different Arp2/3 complex perturbations. (*J*) Quantification of indentations depths of VCA-expressing ACs and *wsp-1*-deleted ACs subjected to *wve-1* RNAi. (*K*) Endogenous GFP-tagged WSP-1/N-WASP and endogenous tagRFP-tagged WVE-1/WAVE are present in the AC at the invasive cell membrane at the P6.p 2-cell and 4-cell stage, colocalized with Lifeact-BFP expressed in the AC. Red arrowheads in *K* indicate spots of colocalization of WSP-1/N-WASP and WVE-1/WAVE signal. (*L*) Colocalization of WSP-1/N-WASP and WVE-1/WAVE at the AC invasive membrane is also observed in the merge (white indicates colocalization), and the coincidence of peaks in the linescans. (*M*) Correlation coefficients to quantify colocalization along the AC invasive membrane at the P6.p 4-cell stage, at a non-AC cell-cell junction in the vulval tissue and in a featureless region in the gut where colocalization can be presumed to be noise (n = 17). (*B*, *C*, and *I*) Epifluorescence microscopy. (*H*, *K*, and *L*) Spinning disk microscopy. (Scale bars, 5 μm.)

indenting into the P6.p daughters were not observed at other locations in the tissue, indicating that BM indentation was a particularity of the AC (*SI Appendix*, Fig. S1). To see whether indentation depth was affected by changes in actin polymerization, we examined the AC/BM-VPC interface in WSP-1/N-WASP-deleted worms. N-WASP is an activator of the Arp2/3 complex, an actin nucleation factor, and a known player in actin assembly for cancer cell invasion (11). In *C. elegans*, WSP-1 is the sole homolog of N-WASP (12), and in the absence of *wsp-1*, most ACs fail to invade by the P6.p 4-cell stage invasion (13). In WSP-1/N-WASP-deleted worms, the AC indentation depth was reduced by ∼50% to 0.6 ± 0.2 μm ($n = 17$), and the actin patch at the AC invasive membrane was halved in area compared with WT [8 ± 3 μm^2 ($n = 36$) versus 4 ± 1 μm^2 ($n = 17$)], although the actin density of the patch was not affected (Fig. 1 *C*–*F*).

From the correlation of indentation depth with actin presence, it seemed possible that actin in the AC was exerting force to create the observed deformation. To determine whether the BM or the underlying VPCs were exerting the counter force, we weakened the BM by depleting collagen IV with RNAi against *emb-9* (a subunit of collagen IV), or by overexpressing secreted protein acidic and rich in cysteine (SPARC), a collagen-binding protein whose overexpression has been shown to decrease levels of collagen IV in BM, leading to enhanced invasion (14). Neither treatment increased the indentation depth under the AC (*SI Appendix*, Fig. S2), so we concluded that the counter force to AC indentation was the VPC epithelial layer.

Given this result and the cone shape of the indentation, the force applied by the AC was estimated using the rigid cone indenter model, where the exerted force was proportional to the elastic modulus (Young's modulus) E of the VPC layer and the square of the indentation depth δ, as expressed by the equation (15): $F = \frac{2}{\pi} tan\alpha \frac{E}{1-\nu^2} \delta^2$. The term $tan\alpha$ is the tangent of the cone semiangle α, and the Poisson ratio ν is taken as 0.5 as per usual for soft materials such as cells (16). The elastic modulus of noncancerous epithelial cell layers, such as the VPCs, is on the order of 10 kPa (17, 18). With these values and the indentation depths and cone angles obtained for individual ACs, we calculated an average of 33 ± 11 nN ($n = 36$) as the force exerted by the AC just before BM penetration (Fig. 1*G*). This estimation is in line with measurements of force production by cellular protrusions such as the lamellipodia of moving cells, which exert tens of nanonewtons of force (19, 20). In contrast, the amount of force applied by the WSP-1/N-WASP-deleted AC was estimated at only 14 ± 5 nN ($n = 17$; Fig. 1*G*). The fact that the force was reduced in WSP-1/N-WASP-deleted worms, which displayed a smaller indentation, less actin at the invasive membrane, and inefficient invasion, implied that actin assembly in the AC applied force to the underlying tissue, deforming and stretching the BM in the process, and possibly helping to break through it.

AC Force Production and Invasion Depends on the Arp2/3 Complex. The involvement of WSP-1/N-WASP and F-actin in AC invasion indicated a role for Arp2/3 complex-based nucleation in AC invasion. RNAi-mediated reduction of *arx-2*, the sole Arp2 subunit of the Arp2/3 complex in the *C. elegans* genome (21), resulted in a nearly 50% defect in AC invasion at the P6.p 4-cell stage (only 54% full invasion; $n = 41$; *SI Appendix*, Fig. S3 for scoring criteria and Table S1).

The stability of the Arp2/3 complex in worms and mammals reduces the efficiency of RNAi for knocking down Arp2/3 complex levels (22, 23). Therefore, to determine the effect of more complete Arp2/3 complex reduction in function, we employed a dominant negative approach: cytosolic expression of the VCA domain of N-WASP to sequester the Arp2/3 complex away from the membrane (24). Expression of VCA from WSP-1 specifically in the AC completely blocked invasion at the P6.p 4-cell stage, 0% full invasion ($n = 30$; Fig. 1*H* and *SI Appendix*, Table S1), and for later-stage animals as well (*SI Appendix*, Fig. S4). Furthermore, at the 2-cell stage, where we see force production in WT worms, we observed that VCA expression reduced actin accumulation at the AC invasive membrane and flattened the AC/VPC interface to an average indentation depth of 0.4 ± 0.4 μm ($n = 17$), with the interface often being completely smooth (Fig. 1 *I* and *J*). The average indentation depth in VCA-expressing ACs was significantly smaller than that of WSP-1/N-WASP-deleted ACs ($P = 0.02$). We concluded that AC invasion was dependent on Arp2/3 complex-based actin nucleation, which produced force for tissue deformation and BM invasion.

The drawback of the genetic perturbations of Arp2/3 complex activity described up until now was that these treatments could interfere with AC morphology at an early stage, leading to incorrect protrusion formation and indirectly affecting later AC force production. To test this, we inhibited the Arp2/3 complex after the formation of the nascent protrusion by applying the small molecule inhibitor of the Arp2/3 complex, CK666. CK666 treatment flattened the AC/VPC interface even though the nascent protrusion did not completely disappear, and this was not observed with the DMSO control (Fig. 1*I*). This result was consistent with perturbations of Arp2/3 complex activity being the direct cause of a decrease in AC indentation depth, and therefore force production.

WVE-1/WAVE Plays a Role in AC Force Production and Invasion. WSP-1/N-WASP deletion reduced actin polymerization in the AC and decreased indentation depth; however, 18% of the worms still displayed complete BM invasion at the P6.p 4-cell stage (*SI Appendix*, Table S1), and 100% of WSP-1/N-WASP-deleted worms succeeded in performing delayed invasion by the P6.p 8-cell stage. In contrast, delayed invasion only rarely occurred with VCA-expressing ACs, as mentioned earlier. Taken together, these data suggested that another regulator could activate the Arp2/3 complex for AC invasion in the absence of WSP-1/N-WASP.

It seemed likely that WAVE, another Arp2/3 complex activator, might play this role. When WSP-1/N-WASP-deleted worms were treated with RNAi targeting *wve-1*, invasion at the P6.p 4-cell stage was reduced to 5% (*SI Appendix*, Table S1). At the 2-cell stage, *wve-1* RNAi in WSP-1/N-WASP-deleted worms gave ACs that resembled VCA-expressing ACs: reduced actin accumulation at the AC invasive membrane and a flattened AC/VPC interface with an average indentation depth of 0.3 ± 0.3 μm ($n = 10$; Fig. 1 *I* and *J*). The interface was sometimes flat, and the difference with WSP-1/N-WASP-deleted worms was significant ($P = 0.009$). In contrast, WVE-1/WAVE deletion on its own showed almost no defect in AC invasion at the P6.p 4-cell stage (*SI Appendix*, Table S1). These results suggested that Arp2/3 complex activation in the AC for invasion was strongly dependent on WSP-1/N-WASP, and less so on WVE-1/WAVE, but that WVE-1/WAVE could compensate partly in activating the Arp2/3 complex after loss of WSP-1/N-WASP.

Endogenous N-WASP and WAVE Colocalize at the AC Invasive Membrane. If both WSP-1/N-WASP and WVE-1/WAVE were participating in AC actin protrusion formation, they should colocalize at the AC invasive membrane. We examined the localization of WSP-1 and WVE-1, using fluorescently labeled worm strains created by CRISPR/Cas-9 genome editing (23). We observed that WSP-1/N-WASP was present at the AC invasive membrane before and after invasion, although it was also visible at cell junctions elsewhere in the vulval and uterine cells (Fig. 1*K*). WVE-1/WAVE was faint overall, but visible in the AC and localized to the invasive membrane before and after invasion (Fig. 1*K*). Spots of WSP-1/N-WASP on the invasive membrane colocalized with spots of WVE-1/WAVE (red arrows Fig. 1*K*). This was further illustrated by merging the channels and

performing a linescan analysis (Fig. 1*L*). To quantify this, we measured the correlation between red and green pixel values in merged images. The two proteins colocalized at the invasive membrane at the 2-cell stage and the 4-cell stage ($r = 0.80$ and 0.84, respectively; Fig. 1*L*), and this was true on average, as well ($r = 0.73 \pm 0.09$, where $r = 1$ indicates perfect colocalization; Fig. 1*M*). Such correlation values were not observed at other cell junctions near the AC or in the gut (Fig. 1*M*). This analysis showed that WVE-1/WAVE was colocalized with WSP-1/N-WASP at the AC invasive membrane.

AC Invasion Does Not Depend on Formins and Actin Filament Crosslinkers. In studies on mammalian cells, when the Arp2/3 complex is inhibited by the VCA approach, lamellipodia collapse, but actin structures that are dependent on alternative nucleators such as formins become more pronounced (22, 25, 26). Here the fact that the VCA-expressing AC did not display actin spikes or other unbranched structures (Fig. 1*H*) suggested that formins were not active in the AC. To examine more closely the role of formin, we evaluated invasion in individual deletions of all six known *C. elegans* formins, as well as in a double and a triple ablation. All perturbations showed WT invasion at the P6.p 4-cell stage (*SI Appendix*, Table S1). These results, together with the absence of protrusive structures in ACs expressing VCA, suggested that formins did not play a role in actin assembly in the AC.

Furthermore, actin filament cross-linkers did not appear to play a role. The *C. elegans* genome lacks fascin, but contains one copy of α-actinin, ATN-1, filamin, FLN-1, and plastin/fimbrin, PLST-1. Individual null mutants (*atn-1*, *plst-1*, and *fln-1*) showed no significant invasion defects, nor did a triple invalidation (*atn-1; plst-1; fln-1* RNAi) (*SI Appendix*, Table S1). It has been shown that entanglement resulting from a high degree of branching can provide cohesion in an actin network despite the absence of cross-linkers (27, 28). RESOLFT superresolution microscopy indicated that the actin network in the AC protrusion was very tightly packed (*SI Appendix*, Fig. S5), and perhaps this was the reason why additional cross-linking was unnecessary.

WSP-1/N-WASP Promotes Dynamic Invasive Protrusion Formation. To understand the effect of activator deletion on actin dynamics in the AC, we imaged F-actin in the AC over time during WT and WSP-1/N-WASP-deleted AC invasion, which occurred with a delay (Movies S1 and S2). We observed that, concomitant with hole opening in the BM, the projected area (z-projection) of the protrusion grew over time in the WT case, attaining a plateau of 13 ± 3 μm^2, whereas the projected area of the WSP-1/N-WASP-deleted AC protrusion remained almost static at an area of 7 ± 1 μm^2 (Fig. 2 *A–C* and *E*). In addition, WT protrusions were more dynamic, and even when the invasive protrusion had reached its maximal area, WT protrusions continued to fluctuate with an average unshared area over time of 3.3 ± 1.0 μm^2/min, whereas WSP-1/N-WASP-deleted protrusions fluctuated less, with an average shape change of 2.1 ± 0.3 μm^2/min (Fig. 2 *D* and *F*). Overall AC protrusions in the absence of N-WASP were smaller and less dynamic than in the WT case, and this correlated with less efficient invasion. Consistent with its minor effect on invasion, loss of WVE-1/WAVE on its own via *wve-1* RNAi did not change the average area of the invasive F-actin protrusion compared with the RNAi control (Fig. 2*G*). Together, these results provided further support for a dominant role of WSP-1/N-WASP in AC invasion, with an accessory role for WVE-1/WAVE.

VCA(WSP-1/N-WASP) Is More Effective than VCA(WVE-1/WAVE) in Activating the Arp2/3 Complex in Vitro. The RhoGTPases, MIG-2/Rac, CED-10/Rac, and CDC-42/Cdc-42, which activate both WSP-1/N-WASP and WVE-1/WAVE, have been shown to be

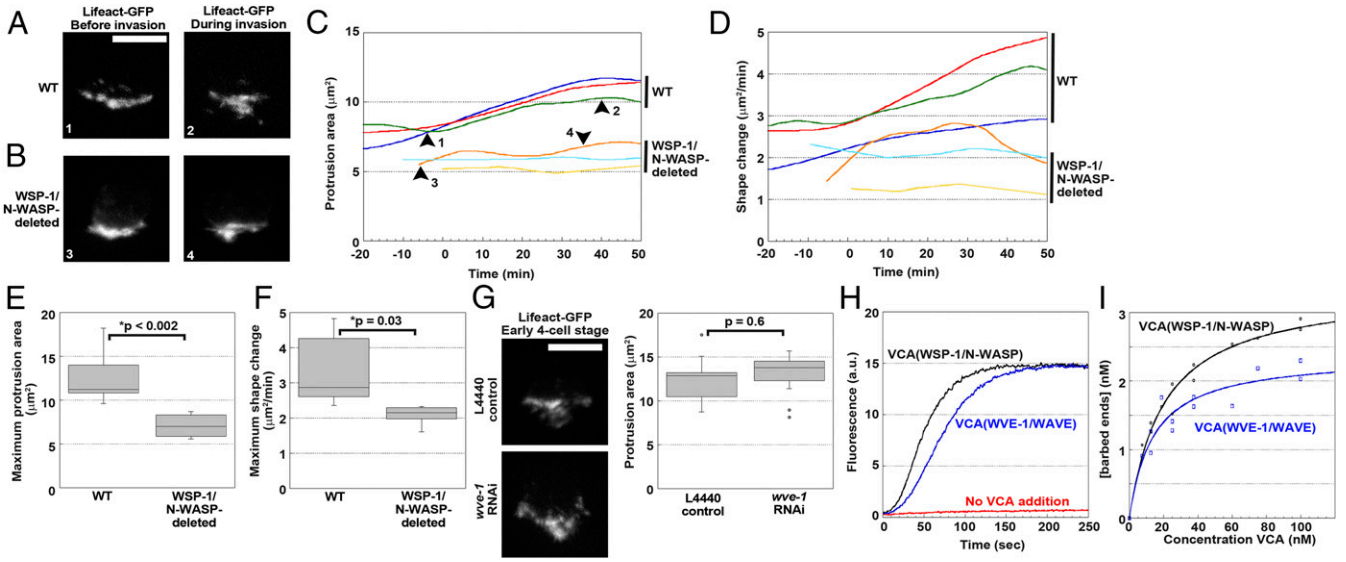

Fig. 2. WSP-1/N-WASP contributes more to actin dynamics in the invasive protrusion than WVE-1/WAVE. Time course of the growth in projected area (maximum intensity projection) of the AC actin protrusion in WT worms (*A* and *C*) and WSP-1/N-WASP-deleted worms (*B* and *C*). Growth curves in (*C*) are aligned with 0 min as the approximate time of first BM breach, as judged either by examining laminin-mCherry signal or by observing an actin protrusion that extends beyond the BM. Each curve represents a worm. The images in *A* and *B* are taken from the curves at the places indicated by the black arrowheads on the green curve and orange curve, respectively, and the number labels are indicated on the images. (*D*) Shape change of the protrusion is evaluated by measuring the unshared area between consecutive frames of the time-lapse movies and normalizing by the acquisition rate. The shape change curves are depicted in the same color as the respective growth curves in *C*. (*E* and *F*) Quantification of the maximum protrusion area and shape change for WT and WSP-1/N-WASP-deleted worms ($n \geq 6$). (*G*) Representative images and quantification of projected areas of the actin protrusion under control RNAi (L4440) and WVE-1/WAVE knockdown ($n \geq 9$). (*H*) Pyrene actin polymerization curves. Both VCA(WSP-1/N-WASP) and VCA(WVE-1/WAVE) are at 100 nM. (*I*) The concentration of barbed ends formed is shown as a function of concentration in VCA. The curves are fit to a Michaelis-Menton curve to obtain the plateaus. (*A*, *B*, and *G*) Spinning disk microscopy. (Scale bars, 5 μm.)

present at the invasive membrane of the AC (13, 29–31). Furthermore, knocking down these RhoGTPases in different combinations with *wsp-1* or *wve-1* deletion was consistent with cooperation between WSP-1/N-WASP and WVE-1/WAVE, with a dominant role for WSP-1/N-WASP (*SI Appendix*, Fig. S6). In this context, it was not clear why WSP-1/N-WASP played a more important role in AC invasion than WVE-1/WAVE. One possibility was that WVE-1/WAVE was less effective in activating the Arp2/3 complex in comparison with WSP-1/N-WASP. To evaluate this, a pyrene-actin assay to measure the formation of F-actin over time was performed using the VCA domains purified from *C. elegans* WSP-1/N-WASP and WVE-1/WAVE in the presence of the Arp2/3 complex.

VCA(WSP-1/N-WASP) was 40% faster at reaching the plateau than VCA(WVE-1/WAVE) at identical concentrations (Fig. 2*H*). The number of filament barbed ends can be calculated using the slopes at half-maximum of such polymerization curves (32). The number of barbed ends formed by each activator in the presence of Arp2/3 complex as a function of VCA concentration showed that VCA(WSP-1/N-WASP) created 1.4-fold more barbed ends: at saturating VCA, VCA(WSP-1/N-WASP) created 3.4 ± 0.1 nM barbed ends, whereas VCA(WVE-1/WAVE) created 2.4 ± 0.2 nM (Fig. 2*I*). This difference in activity could explain why WVE-1/WAVE played a lesser role in AC invasion compared with WSP-1/N-WASP.

Perturbing WSP-1/N-WASP Function Does Not Alter AC Polarity, Trafficking of Invasive Membrane, or Secretion. It was possible that the strong defect in AC invasion we observed on interfering with WSP-1/N-WASP activity derived from an effect on polarity maintenance, trafficking, or secretion in the AC, as actin filaments are implicated in different aspects of all these processes. As a polarity marker, we examined UNC-40/DCC, the UNC-6/netrin receptor in the AC key for invasion, known to be threefold enriched at the invasive membrane compared with the apical and lateral membranes (29, 30). Polarity of UNC-40/DCC was unaffected by *wsp-1* RNAi (Fig. 3 *A* and *B*).

The AC invasive membrane is also rich in $PI(4,5)P_2$, which is recycled via endomembrane compartments (29, 33). Exocytosis of endomembranes via SNARE proteins and the exocyst is thought to supply membrane to the growing invasive protrusion in the AC (34). When trafficking of intracellular vesicles is impeded, for example, when nondynamic actin accumulates in the AC because of ADF/cofilin disruption, $PI(4,5)P_2$-rich vesicles accumulate in the cytoplasm, invasive membrane $PI(4,5)P_2$ is reduced, and invasion does not occur properly (33). We evaluated whether trafficking was being affected in our reduced WSP-1/N-WASP conditions by measuring the amount of $PI(4,5)P_2$ in the invasive membrane compared with the amount in the cytoplasm, using a fluorescently labeled PH construct that binds $PI(4,5)P_2$. We performed a similar analysis for a reporter of ZMP-1, a metalloprotease implicated in digestion of the BM for AC invasion and trafficked to the AC invasive membrane in $PI(4,5)P_2$-positive compartments (9, 10, 34). The percentage of $PI(4,5)P_2$ and ZMP-1 signal found at the invasive membrane was the same in control and *wsp-1* knockdown conditions (Fig. 3 *C*–*F*), indicating that localization of invasive components to the AC invasive membrane was occurring normally in reduced *wsp-1* conditions where invasion was blocked. ZMP-1 was also correctly localized when invasion was drastically blocked via VCA expression (*SI Appendix*, Fig. S7). This showed that proteases on their own were not sufficient for invasion, as VCA-expressing ACs almost never pierced the BM, unlike WSP-1/N-WASP knockdown worms, which showed delayed invasion.

To probe secretion, we looked at HIM-4/hemicentin, an extracellular matrix molecule secreted by the AC during invasion (10, 29). In WT conditions, HIM-4/hemicentin forms punctate structures beneath the invading AC, whereas when secretion is disrupted by interfering with netrin/UNC-6 signaling, for example, HIM-4/hemicentin is retained in the AC and fewer puncta form (10, 29). RNAi against *wsp-1* did not affect the deposition

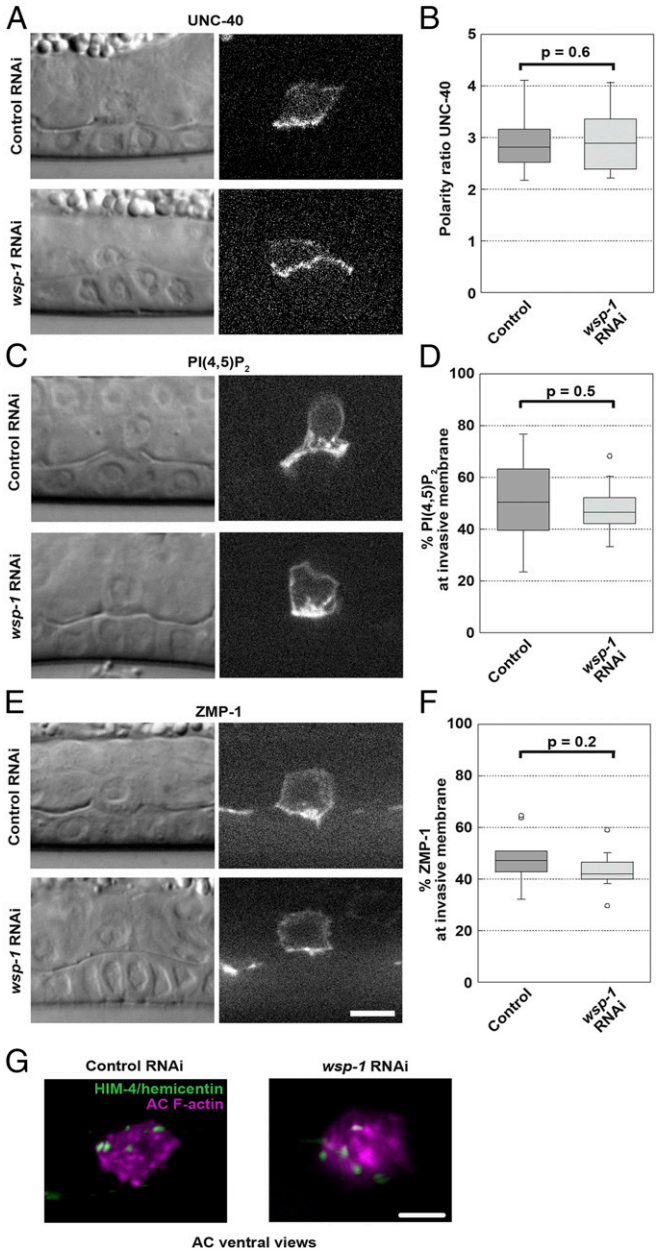

Fig. 3. WSP-1/N-WASP deletion does not affect AC polarity, trafficking of invasive membrane or secretion. Single plane images of worms at the P6.p 4-cell stage coupled with DIC images are shown, treated with an RNAi control (L4440) or treated with *wsp-1* RNAi to knock down WSP-1/N-WASP. Only those *wsp-1* RNAi samples that show a complete block at the 4-cell stage are evaluated. (*A*) Representative images of the polarity marker UNC-40-GFP in control RNAi and *wsp-1* RNAi conditions. (*B*) Quantification of the polarity factor (*SI Appendix, Supplemental Methods*). $n \geq 18$. (*C* and *E*) Representative images of the invasive membrane markers, $PI(4,5)P_2$ (mCherry-PH) and ZMP-1 (GFP-ZMP-1-GDI) are shown in control RNAi and *wsp-1* RNAi conditions. (*D* and *F*) Quantification of the percentage of the total fluorescent signal found at the invasive membrane for $PI(4,5)P_2$ and ZMP-1 (*SI Appendix, Supplemental Methods*). $n \geq 12$. (*G*) Ventral view images of animals treated with control RNAi (*Left*) or *wsp-1* RNAi (*Right*) display similar deposition of HIM-4/hemicentin-GFP under the AC footprint (magenta, F-actin). Ventral views are used to better visualize HIM-4/hemicentin puncta underneath the AC. Images are representative of 20 animals examined. Spinning disk microscopy. (Scale bars, 5 μm.)

of HIM-4/hemicentin puncta underneath the AC (Fig. 3*G*). All together, these results suggested that the invasion defect observed in WSP-1/N-WASP-deleted worms was not the result of a defect in AC polarity, trafficking of invasive membrane, or secretion, but rather, decreased actin dynamics in the invasive protrusion and decreased force production, confirming an active role for actin polymerization in BM invasion.

Concluding Remarks

Forces are exerted by cancer-associated fibroblasts to facilitate cancer cell passage across BM (35). However, it remains unclear whether mechanical forces produced by the invading cell itself are equally important. Here we show that the invading AC forms a large actin network via the activity of the Arp2/3 complex, downstream of both WSP-1/N-WASP and WVE-1/WAVE. This protrusion deforms the underlying matrix/tissue, potentially applying a mechanical stretch to the BM that could help tear BM fibers apart. Indeed, we link deformation and force production to invasion efficiency, demonstrating that actin-based cell mechanics play a role in BM invasion, consistent with previous suppositions (31). Proteases also contribute to the AC invasion process, and the interplay between actin assembly and protease activity is the subject of ongoing work. In conclusion, we provide evidence that actin-based force production by an invading cell in *C. elegans* is a determining factor for driving invasion.

Methods

Worm strains, plasmid constructs, worm handling, CK666 treatment, imaging and analysis, protein purification, the pyrene assay, and RESOLFT microscopy are described in the *SI Appendix*. Briefly, *C. elegans* worms were manipulated and mounted for imaging as described (36). Imaging was performed on a spinning disk confocal or an epifluorescence microscope, as noted in figure legends. Analysis was performed using Metamorph or ImageJ software. All data are represented as averages ± SD. Statistical comparison of means was done by the Student *t* test, and *P* values are reported. Statistical comparison of proportions (percentage in the RNAi experiments) was done using the χ^2 test, and *P* values are reported. A *P* value of 0.05 or less is considered significant.

ACKNOWLEDGMENTS. We warmly acknowledge the Cell and Tissue Imaging Platform (member of France–BioImaging, ANR-10-INBS-04) of the Genetics and Developmental Biology Department (UMR3215/U934) of Institut Curie for help with light microscopy. We thank Fabrice Cordelières (Université de Bordeaux) for help with Metamorph/Image J cross-talk, and Ranjay Jayadev (Duke University) for discussions about the SPARC overexpression and *emb-9* RNAi experiments. J.P. acknowledges financial support from the Fondation pour la Recherche Médicale (Grant DEQ20120323737) and the Fondation ARC (Grant PJA 20151203487). This work also received support under the program "Investissements d'Avenir" launched by the French Government and implemented by ANR (ANR-10-LABX-0038 and ANR-10-IDEX-0001-02 PSL), including financing of N.B. R.C. was funded by a PhD fellowship from ITMO Cancer. D.R.S. was supported by National Institute of General Medical Sciences (R01 GM079320 and Maximizing Investor's Research Award R35 GM118049), and National Institute of Child Health and Human Development (R21 HD084290). J.D. thanks the Carlsberg Foundation for financial support, and I.T. is supported by the European Research Council Starting Grant Funding scheme (MoNaLISA 638314).

1. Castro-Castro A, et al. (2016) Cellular and molecular mechanisms of MT1-MMP-dependent cancer cell invasion. *Annu Rev Cell Dev Biol* 32:555–576.
2. Nürnberg A, Kitzing T, Grosse R (2011) Nucleating actin for invasion. *Nat Rev Cancer* 11:177–187.
3. Linder S, Wiesner C, Himmel M (2011) Degrading devices: Invadosomes in proteolytic cell invasion. *Annu Rev Cell Dev Biol* 27:185–211.
4. Beaty BT, Condeelis J (2014) Digging a little deeper: The stages of invadopodium formation and maturation. *Eur J Cell Biol* 93:438–444.
5. Yu X, et al. (2012) N-WASP coordinates the delivery and F-actin-mediated capture of MT1-MMP at invasive pseudopods. *J Cell Biol* 199:527–544.
6. Sahai E (2005) Mechanisms of cancer cell invasion. *Curr Opin Genet Dev* 15:87–96.
7. Machesky LM (2008) Lamellipodia and filopodia in metastasis and invasion. *FEBS Lett* 582:2102–2111.
8. Sherwood DR, Plastino J (2018) Invading, leading and navigating cells in Caenorhabditis elegans: Insights into cell movement in vivo. *Genetics* 208:53–78.
9. Matus DQ, et al. (2015) Invasive cell fate requires G1 cell-cycle arrest and histone deacetylase-mediated changes in gene expression. *Dev Cell* 35:162–174.
10. Sherwood DR, Butler JA, Kramer JM, Sternberg PW (2005) FOS-1 promotes basement-membrane removal during anchor-cell invasion in C. elegans. *Cell* 121:951–962.
11. Yamaguchi H, et al. (2005) Molecular mechanisms of invadopodium formation: The role of the N-WASP-Arp2/3 complex pathway and cofilin. *J Cell Biol* 168:441–452.
12. Patel FB, et al. (2008) The WAVE/SCAR complex promotes polarized cell movements and actin enrichment in epithelia during C. elegans embryogenesis. *Dev Biol* 324: 297–309.
13. Lohmer LL, et al. (2016) A sensitized screen for genes promoting invadopodia function in vivo: CDC-42 and Rab GDI-1 direct distinct aspects of invadopodia formation. *PLoS Genet* 12:e1005786.
14. Morrissey MA, et al. (2016) SPARC promotes cell invasion in vivo by decreasing type IV collagen levels in the basement membrane. *PLoS Genet* 12:e1005905.
15. Sneddon I (1948) Boussinesq's problem for a rigid cone. *Math Proc Cambridge Philos Soc* 44:492–507.
16. Guz N, Dokukin M, Kalaparthi V, Sokolov I (2014) If cell mechanics can be described by elastic modulus: Study of different models and probes used in indentation experiments. *Biophys J* 107:564–575.
17. Kuznetsova TG, Starodubtseva MN, Yegorenkov NI, Chizhik SA, Zhdanov RI (2007) Atomic force microscopy probing of cell elasticity. *Micron* 38:824–833.
18. Lekka M, et al. (1999) Elasticity of normal and cancerous human bladder cells studied by scanning force microscopy. *Eur Biophys J* 28:312–316.
19. Abraham VC, Krishnamurthi V, Taylor DL, Lanni F (1999) The actin-based nanomachine at the leading edge of migrating cells. *Biophys J* 77:1721–1732.
20. Brunner CA, et al. (2006) Cell migration through small gaps. *Eur Biophys J* 35:713–719.
21. Sawa M, et al. (2003) Essential role of the *C. elegans* Arp2/3 complex in cell migration during ventral enclosure. *J Cell Sci* 116:1505–1518.
22. Wu C, et al. (2012) Arp2/3 is critical for lamellipodia and response to extracellular matrix cues but is dispensable for chemotaxis. *Cell* 148:973–987.
23. Zhu Z, et al. (2016) Functional coordination of WAVE and WASP in *C. elegans* neuroblast migration. *Dev Cell* 39:224–238.
24. Machesky LM, Insall RH (1998) Scar1 and the related Wiskott-Aldrich syndrome protein, WASP, regulate the actin cytoskeleton through the Arp2/3 complex. *Curr Biol* 8: 1347–1356.
25. Koestler SA, et al. (2013) Arp2/3 complex is essential for actin network treadmilling as well as for targeting of capping protein and cofilin. *Mol Biol Cell* 24:2861–2875.
26. Suraneni P, et al. (2012) The Arp2/3 complex is required for lamellipodia extension and directional fibroblast cell migration. *J Cell Biol* 197:239–251.
27. Achard V, et al. (2010) A "primer"-based mechanism underlies branched actin filament network formation and motility. *Curr Biol* 20:423–428.
28. Dayel MJ, et al. (2009) In silico reconstitution of actin-based symmetry breaking and motility. *PLoS Biol* 7:e1000201.
29. Ziel JW, Hagedorn EJ, Audhya A, Sherwood DR (2009) UNC-6 (netrin) orients the invasive membrane of the anchor cell in *C. elegans*. *Nat Cell Biol* 11:183–189.
30. Hagedorn EJ, et al. (2009) Integrin acts upstream of netrin signaling to regulate formation of the anchor cell's invasive membrane in C. elegans. *Dev Cell* 17:187–198.
31. Hagedorn EJ, et al. (2013) The netrin receptor DCC focuses invadopodia-driven basement membrane transmigration in vivo. *J Cell Biol* 201:903–913.
32. Higgs HN, Blanchoin L, Pollard TD (1999) Influence of the C terminus of Wiskott-Aldrich syndrome protein (WASp) and the Arp2/3 complex on actin polymerization. *Biochemistry* 38:15212–15222.
33. Hagedorn EJ, et al. (2014) ADF/cofilin promotes invadopodial membrane recycling during cell invasion in vivo. *J Cell Biol* 204:1209–1218.
34. Naegeli KM, et al. (2017) Cell invasion in vivo via rapid exocytosis of a transient lysosome-derived membrane domain. *Dev Cell* 43:403–417.e10.
35. Glentis A, et al. (2017) Cancer-associated fibroblasts induce metalloprotease-independent cancer cell invasion of the basement membrane. *Nat Commun* 8:924.
36. Kelley LC, et al. (2017) Live-cell confocal microscopy and quantitative 4D image analysis of anchor-cell invasion through the basement membrane in *Caenorhabditis elegans*. *Nat Protoc* 12:2081–2096.